RSC Advances

PAPER

View Article Online
View Journal | View Issue

Cite this: *RSC Adv.*, 2020, **10**, 5212

Gram-scale synthesis of ultra-fine Cu_2O for highly efficient ozone decomposition

Shuyan Gong,†[ab] Anqi Wang,†[ab] Jilai Zhang,[a] Jian Guan,[a] Ning Han *[abc] and Yunfa Chen *[abc]

Received 26th November 2019
Accepted 10th January 2020

DOI: 10.1039/c9ra09873a

rsc.li/rsc-advances

Nowadays, it is necessary and challenging to prepare Cu_2O in a large scale for various applications such as catalysis due to its excellent properties. Here, gram-scale Cu_2O with nm size is successfully prepared using a simple liquid-phase reduction method at 25 °C. The amount of NaOH is found to be the key factor to determine the particle size of Cu_2O by modifying the complexation and reduction reactions. The obtained ultra-fine Cu_2O exhibits high performance of >95% efficiency for removing high-concentration (3000 ppm) ozone at 25 °C and even at a high relative humidity (RH) of 90% for more than 8 h. Furthermore, the Cu_2O nanoparticles are coated onto an aluminium honeycomb substrate to form a monolithic catalyst, which shows high ozone removal efficiency of >99% in dry air and >97% in 90% RH for >10 h at a space velocity of 8000 h^{-1}. The high performance could be attributed to the enhanced release of the ozone decomposition intermediate by the small size of Cu_2O, as verified by O_2 temperature-programmed desorption and X-ray photoelectron spectroscopy. All these results show the industrial promise of the large scale synthesis of ultrafine Cu_2O applicable for high-performance ozone removal.

1. Introduction

In recent years, ozone pollution has become an emerging issue all over the world;[1] ozone is mainly formed by a series of complex solar-driven reactions between volatile organic compounds (VOCs) and NO_x.[2,3] Moreover, ozone is widely used in industrial wastewater treatment, pulp bleaching, and complete oxidation of exhaust gases due to its high reactivity.[4–6] The off-gas from the ozone contacting chamber usually contains excessive residual ozone. Elevated ozone levels near the ground can have a number of adverse effects on the environment and organisms.[7–9] Ozone can enhance the oxidizing properties of the atmosphere and react with nitrogen oxides to promote the formation of nitrate particles.[10] Moreover, the reaction of ozone with olefins to form hydroxyl radicals plays an important role in photochemical air pollution.[11] Indoor copiers, laser printers, and fax machines also produce low levels of ozone, which reacts with other indoor pollutants to produce secondary pollutants and aerosol particles.[12] The produced secondary emissions of particulate matter may be more harmful to human health than ozone itself. Therefore, it is urgently necessary to develop effective methods to eliminate ozone.

Although ozone is thermodynamically unstable, it decomposes slowly below 523 K without a catalyst. Catalytic decomposition has realized the catalytic removal of ozone at 25 °C and has become the focus of current research because of its high decomposition efficiency, safety and economy. The active components of the catalyst mainly include noble metals[13–15] and transition metal oxides.[16–19] Imamura *et al.* reported that p-type semiconductors have higher decomposition efficiency for ozone than n-type semiconductors.[20] Oyama measured the conductivity of the catalyst by the Hall effect and compared the correlation between oxide activity and conductivity, thereby further confirming that the p-type semiconductor oxide has higher activity for the catalytic decomposition of ozone.[21] Cu_2O is a typical p-type semiconductor oxide, and intensive efforts have been focused on the shape and size control of Cu_2O.[22–24] In general, Cu_2O particles with various morphologies can be produced by different synthetic methods, including thermal decomposition,[25] solvothermal synthesis,[26] hydrothermal method,[27] polyol synthesis,[28] seed-mediated chemical deposition,[29] and liquid-phase reduction.[30] It has been found that Cu_2O with a smaller particle size tends to exhibit higher performance for ozone degradation.[31] However, there is still much work to do for the development of the Cu_2O catalyst, particularly in terms of large-scale synthesis and size reduction. For example, for good morphology control, one of the difficulties is the small amount of precursor solutions used for Cu_2O

[a]State Key Laboratory of Multiphase Complex Systems, Institute of Process Engineering, Chinese Academy of Sciences, Beijing 100190, PR China
[b]Center of Materials Science and Optoelectronics Engineering, University of Chinese Academy of Sciences, No. 19A Yuquan Road, Beijing 100049, PR China
[c]Center for Excellence in Regional Atmospheric Environment, Institute of Urban Environment, Chinese Academy of Sciences, Xiamen 361021, PR China
† Shuyan Gong and Anqi Wang contributed equally.

synthesis, which induces a low yield.[32] Another one is the dilution of precursor solutions and the use of surfactants such as oleic acid, poly(vinylpyrrolidone), or sodium dodecyl sulfate, due to which the products need to be thoroughly washed with water and ethanol to remove the residual surfactants and byproducts. This process is not only energy-intensive, but also causes high wastewater emission as the output increases. Therefore, it is urgent and challenging to controllably synthesize Cu_2O with large scale production and high catalytic performance.

In this method, the large-scale synthesis of fine Cu_2O nanoparticles with a production of above 20 grams in an experimental batch is achieved using highly concentrated precursor solutions, which may meet the criteria for practical applications. Importantly, the obtained Cu_2O displays complete removal of ozone to 1000 ppm at 25 °C both in dry flow and high relative humidity levels (*ca.* 90%). The ozone conversion could still be above 99% and 95% in dry flow and RH 90%, respectively, for high-concentration 3000 ppm ozone. Finally, the prepared Cu_2O is processed on an Al honeycomb substrate and exhibits high elimination efficiency and stability for ozone decomposition, which shows great potential for practical applications.

2. Experimental section

2.1 Synthesis of Cu_2O catalyst

The synthesis process was conducted at 25 °C using concentrated precursor solutions in order to obtain high yield and low wastewater emission. First, an NaOH aqueous solution (5 M) with variable volumes was mixed with 500 mL $CuSO_4$ (0.6 M) solution with vigorous stirring. Then, 187.5 mL (1 M) ascorbic acid (AA) solution was injected into the suspension, and the whole content was stirred for about 20 minutes. At last, the as-synthesized material was washed with deionized water and ethanol and then dried in vacuum at 80 °C overnight. The size of Cu_2O was adjusted by adding different volumes of NaOH: 120 mL, 150 mL and 300 mL. The prepared Cu_2O was named by the molar ratio of $CuSO_4$ to NaOH as 1 : 2, 1 : 2.5 and 1 : 5.

Fabrication of Cu_2O–Al honeycomb: 0.2 g Cu_2O powder was slurried in 10 g Al_2O_3 sol. Al honeycomb (1 mm pore and 20 mm thickness) was precipitated in the slurry several times, and the final product was dried at 25 °C in a fume hood. The weight of the Al honeycomb was measured before and after coating, and the active material (defined as the weight of all additives: Al_2O_3 sol and Cu_2O powder) weight was determined by calculating the difference.

2.2 Characterizations

The crystal structure was measured by powder X-ray diffraction (XRD) on a Panalytical X'Pert PRO system (40 kV, 40 mA) with Cu-Kα radiation (0.154 nm) in the diffraction angle (2θ) range of 5–90°. The images of sample morphology and size were obtained on a scanning electron microscope (SEM, JEOL JSM-6700F, Japan, 15 kV, 10 mA) and transmission electron microscope (TEM, JEOL JEM-2100F, 200 kV). The surface atom status was analyzed by X-ray photoelectron spectroscopy (XPS) on an XLESCALAB 250Xi electron spectrometer from VG Scientific with monochromatic Al–Kα radiation. H_2-temperature-programmed reduction (TPR) experiments and O_2-temperature-programmed desorption (TPD) were conducted on an automated catalyst characterization system (Autochem 2920). The detailed processes are as follows: In H_2-TPR, about 50 mg powder (40–60 mesh) was loaded in a U-shaped quartz reactor at a gas flow of 10% H_2 balanced with Ar at 25 mL min^{-1}. The temperature was raised to 750 °C with a rate of 10 °C min^{-1}. In O_2-TPD, 100 mg sample was pre-heated in He flow from 25 °C to 150 °C for 1 h to remove surface adsorbates. After that, the catalyst was cooled and purged with 5% O_2/He at 50 °C and held for 4 h. Desorption of O_2 was carried out from 50 °C to 600 °C at a heating rate of 10 °C min^{-1} in pure He.

2.3 Catalytic activity evaluation

The ozone decomposition performance was measured in a U-shape quartz tube reactor (diameter 5.5 mm) at 25 °C and 50 mg (40–60 mesh) catalyst mixed with 450 mg quartz sand was used in every test. Ozone was generated at 1000 or 3000 ppm by a commercial ozone generator (COM-AD-01-OEM, ANSEROS COMPANY, Anshan, China), and the inlet and outlet ozone concentrations were analyzed by an ozone monitor (model 106M, 2B Technologies, USA). The total space velocity (SV) was 240 000 mL g^{-1} h^{-1} with a total gas flow of 200 mL min^{-1}. The ozone conversion was calculated as $100\% \times (C_{inlet} - C_{outlet})/C_{inlet}$. The test of moisture-resistance properties was produced by bubbling water with the airflow, and the relative humidity (RH) was measured by a humidity and temperature sensor meter (center 310 RS-232, TES, Taiwan).

3. Results and discussion

3.1 Crystal structure, morphology, and formation mechanism of prepared samples

Fig. 1a shows the XRD patterns of the prepared samples; all the XRD peaks can be indexed to the pure phase Cu_2O (cuprites, JCPDS no. 003-0898) without the presence of any impurities. It was noted that the main peaks of the Cu_2O-1 : 2 and Cu_2O-1 : 2.5 samples became broader compared with that of Cu_2O-1 : 5 (Fig. 1b), which indicated a smaller particle size. Fig. 2 exhibits the SEM, TEM, and HRTEM images of the three samples, from which we can see that all the samples appear to contain the stacking of nanometric particles due to the small size. The particle size of Cu_2O-1 : 5 was about 100 nm, and the particle sizes of Cu_2O-1 : 2 and Cu_2O-1 : 2.5 were below 50 nm. Moreover, it was noticed that the nanoparticles of Cu_2O-1 : 2.5 were composed of even smaller particles with a size of just several nanometers (Fig. 2e and inset), which was in good agreement with the broadened XRD pattern. The measured particle lattice fringe of about 0.212 nm (as shown in Fig. 2g–i) corresponds to the interplanar distance of the (200) facet in Cu_2O.[24] The grain sizes calculated by the Scherrer equation and the specific surface areas of the three samples are listed in Table 1. It shows that Cu_2O-1 : 2.5 presents the smallest grain size of

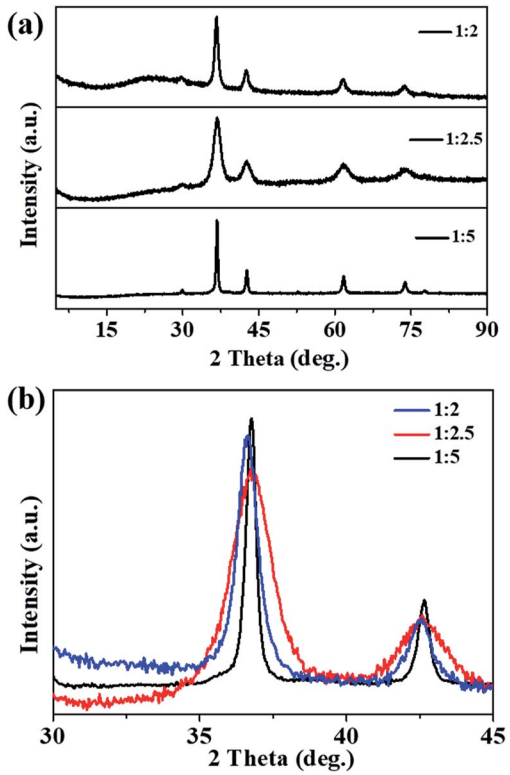

Fig. 1 (a) Powder XRD patterns and (b) high-resolution XRD of the main peak of prepared Cu_2O samples.

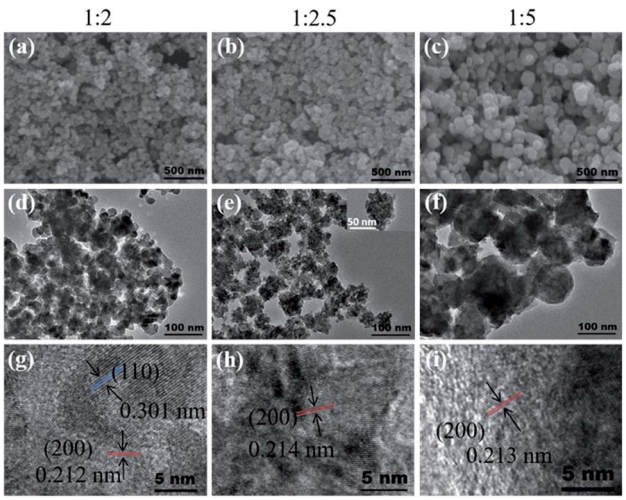

Fig. 2 (a–c) SEM, (d–f) TEM and (g–i) HRTEM images of prepared Cu_2O samples.

about 5.1 nm and the corresponding largest specific surface area of 42.7 $m^2 g^{-1}$.

The ratio of OH^-/Cu^{2+} is the key to control the size of Cu_2O by modifying the complexation and reduction reactions. On one hand, OH^- could act as a ligand to complex with Cu^{2+} cations, forming dependent precursors. The SEM images and XRD patterns of the precursors obtained at different molar ratios of $CuSO_4$ and NaOH are shown in Fig. 3. The nanosheet-shaped

Table 1 Specific surface area and grain size of prepared samples

Catalysts	Specific surface area ($m^2 g^{-1}$)	Grain size (nm)
1 : 2 Cu_2O	37.2	10.9
1 : 2.5 Cu_2O	42.7	5.1
1 : 5 Cu_2O	18.9	21.1

$CuSO_4(OH)_6$ precursor was formed due to an insufficient amount of the OH^- ligand when the ratio of $CuSO_4$ and NaOH was 1 : 2, as shown in Fig. 3a and d, while the $Cu(OH)_2$ nanowire precursor was formed when the ratio of $CuSO_4$ and NaOH increased to 1 : 2.5 and 1 : 5 (verified from Fig. 3b–d). The different precursors produced have different redox potentials, having an effect on the reaction thermodynamics. On the other hand, a highly alkaline solution can improve the reaction rate of the reducing agent AA.[33,34] The reduction rate was slow in the condition of 1 : 2 due to the consumption of OH^- by complexation; thus, the Cu_2O nuclei gradually grew to form a small-size Cu_2O monomer. In contrast, some $Cu(OH)_4^{2-}$ precursor species may be produced under the ratio of 1 : 5 (although $Cu(OH)_4^{2-}$

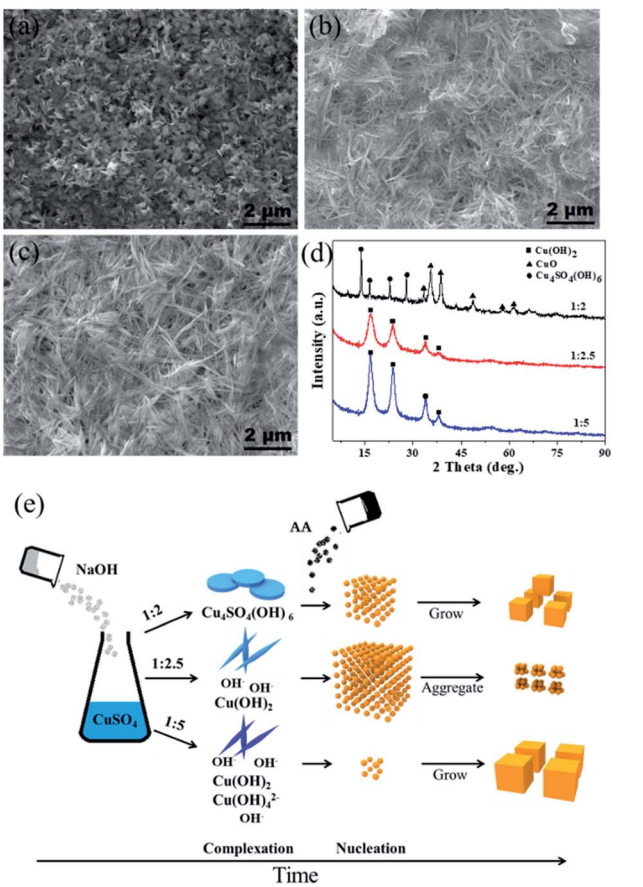

Fig. 3 (a–c) SEM images of precursors obtained at different molar ratios of $CuSO_4$ and NaOH as 1 : 2, 1 : 2.5 and 1 : 5; (d) XRD of precursors obtained at different molar ratios of $CuSO_4$ and NaOH as 1 : 2, 1 : 2.5 and 1 : 5; (e) schematic of Cu_2O formation process under different molar ratios of $CuSO_4$ and NaOH.

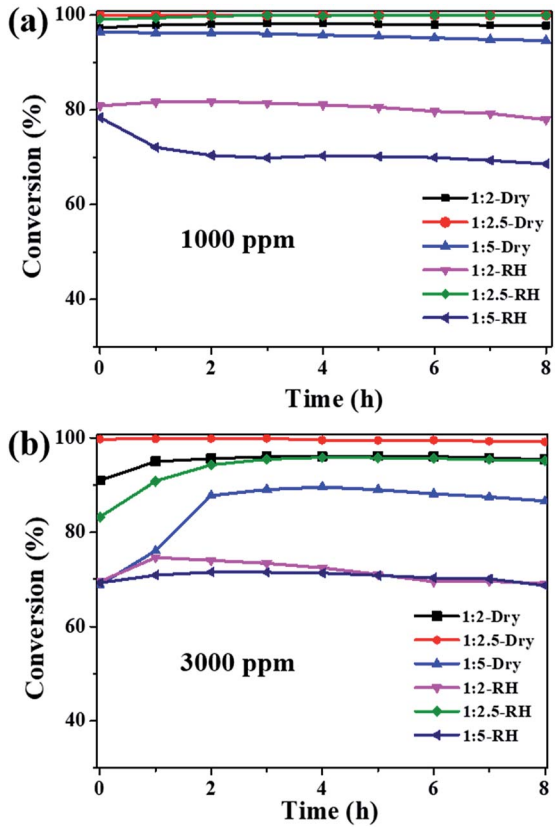

Fig. 4 The conversion of ozone on obtained Cu_2O catalysts: (a) ozone inlet concentration of 1000 ppm; (b) ozone inlet concentration of 3000 ppm ($T = 25$ °C, SV = 240 000 mL g^{-1} h^{-1}, dry air or RH ~ 90%).

cannot be detected by XRD, it can be speculated by the color change of the reaction system from a blue $Cu(OH)_2$ precipitate (1 : 2.5) to a deep blue $Cu(OH)_4^{2-}$ solution (1 : 5)), which will decrease the redox potential; thus, few nuclei are formed, leading to the formation of Cu_2O with a large size. Theoretically, there should be a suitable amount of OH^- to balance the complexation and reduction reactions. Combined with the experimental results, we infer that the $Cu(OH)_2$ nanowire precursor is mainly formed when the ratio is 1 : 2.5; at the same time, the reduction reaction rate is relatively high due to a suitable alkaline environment. As a result, a large amount of the Cu_2O nuclei are formed instantly and cluster to reduce the surface energy, forming aggregated ultrafine nanoparticles. A schematic of the Cu_2O formation process under different amounts of NaOH is shown in Fig. 3e.

3.2 Catalytic activity evaluation of prepared samples

The ozone catalytic performances of the as-synthesized samples (1 : 2, 1 : 2.5 and 1 : 5) were tested at 25 °C in dry and high humidity conditions. Fig. 4a shows that all the three samples exhibit high catalytic activities for 1000 ppm ozone in dry flow, with the ozone conversion efficiency in the sequence of Cu_2O-1 : 2.5 (100%) > Cu_2O-1 : 2 (97.5%) > Cu_2O-1 : 5 (94.6%). Water vapor is known to have a negative impact on the ozone catalytic activity; the ozone conversions over Cu_2O-1 : 2 and Cu_2O-1 : 5 dropped to 77.9% and 68.6%, respectively, at 90% RH. However, the ozone conversion over Cu_2O-1 : 2.5 was still nearly 100% after the 8 h test under the high RH of 90%. These results suggest that particle size has a great influence on ozone catalytic activity, and Cu_2O-1 : 2.5 shows complete conversion for 1000 ppm ozone both in dry and high humidity conditions at 25 °C. To explore more about the activity, the ozone concentration of 3000 ppm was introduced; the decomposition efficiency is shown in Fig. 4b. For the Cu_2O-1 : 2 and Cu_2O-1 : 5 catalysts, the ozone conversion has different degrees of decline either under dry or high humidity conditions due to the high

Table 2 Ozone catalytic decomposition comparison of the catalysts in this study and in publications

Catalyst	Conc.[a] (ppm)	RH[b] (%)	SV[c] (mL g^{-1} h^{-1})	S_{BET}[d] (m^2 g^{-1})	Conv.[e] (%)	Rate (mmol g^{-1} h^{-1})	SA[f] (mmol m^{-2} h^{-1})
MnO_2	120	50	600 000	90	63	2.0	2.3×10^{-2}
MIL-100(Fe)	45	45	200 000	1726	100	0.4	2.3×10^{-3}
Ce-OMS-2	40	90	600 000	200	90	0.96	4.8×10^{-3}
α-MnO_2	14	~1	660 000	80.7	100	0.41	5.1×10^{-3}
α-MnO_2	50	22	540 000	52.4	99	1.2	2.3×10^{-2}
		70			25	0.3	5.8×10^{-3}
H-MnO_2	120	50	600 000	228	60	1.9	8.5×10^{-3}
H-δ-MnO_2	3000	Dry	600 000	206	100	80	3.9×10^{-1}
$MnFe_{0.5}O_x$	10 000	90	12 000	262	90	4.8	1.8×10^{-2}
MnO_x	1000	Dry	120 000	116.2	98.5	5.3	4.5×10^{-2}
CoO_x	1000	Dry	120 000	67.0	88.1	4.7	7.0×10^{-2}
Ag-H-MCM	4400	Dry	114 000	574	97.8	22	3.8×10^{-2}
$LaFe_{0.95}Ni_{0.05}O_3$	1000	Dry	240 000	18.7	97.7	10	5.3×10^{-1}
		RH			93	9.9	5.3×10^{-1}
Cu_2O-1 : 2.5	1000	Dry	240 000	26.5	100	10.7	4×10^{-1}
		90			100	10.7	4×10^{-1}
Cu_2O-1 : 2.5	3000	Dry	240 000	26.5	100	32	1.2
		90			95	31	1.17

[a] Ozone initial concentration. [b] Relative humidity. [c] Space velocity. [d] Specific surface area determined by BET method. [e] Ozone conversion. [f] Surface specific catalytic activity.

concentration. However, Cu_2O-1 : 2.5 still maintains the best catalytic efficiency for 3000 ppm ozone, and the ozone conversion is 99.2% in dry flow. Importantly, water vapor has little effect on the activity, and ozone conversion is above 95% under 90% RH, showing its promise for dealing with high-concentration and high-humidity ozone. The catalytic activity of Cu_2O-1 : 2.5 is compared with those of some recently reported catalysts (Table 2).[35–45] It is noted that the reaction rate (mol g^{-1} h^{-1}) of Cu_2O-1 : 2.5 is one of the highest in the list, especially under high humidity. In order to make a more reasonable comparison, the reaction rate is normalized to the catalyst specific area, *i.e.*, the surface-specific catalytic rate (SA, the number of moles of decomposed ozone per square meter per hour, mol m^{-2} h^{-1}). It is obvious that the SA of Cu_2O-1 : 2.5 is 1–2 orders of magnitude higher than those of the other published catalysts, suggesting its high intrinsic catalytic activity for ozone removal. It should be noted that there are no mesopores in ultrafine Cu_2O and thus, water vapor can only be adsorbed/desorbed on the surface, which would account for the high humidity resistivity as compared with that of the large-surface-area porous oxide catalyst reported in the literature.

3.3 TPR and TPD analyses

The reducibility of the three samples was investigated by H_2-TPR, as shown in Fig. 5a. Cu_2O-1 : 5 exhibited the main reduction peaks located at 260 °C and 275 °C, which could be assigned to the reduction of the Cu_2O species.[46] It was noted that the dominant reduction peaks of Cu_2O-1 : 2 and Cu_2O-1 : 2.5 were observed at around 220 °C, and the second peak was located at about 260 °C. In particular, for Cu_2O-1 : 2.5, most of the reduction occurred at the lowest temperature of 220 °C. This result suggests that the position of the reduction peak is strongly related to the particle size and Cu_2O-1 : 2.5 has the highest reducibility. The easier redox property of Cu_2O-1 : 2.5 may be helpful for its catalytic properties for ozone decomposition.

O_2-TPD was conducted to explore the evolution of oxygen (Fig. 5b). The peak occurring below 100 °C is usually attributed to the desorption of physically adsorbed oxygen, and the peak at higher temperatures (<400 °C) can be ascribed to the release of chemically adsorbed oxygen.[47,48] Evidently, the strongest oxygen desorption peak was observed in the O_2-TPD profile of Cu_2O-1 : 2.5 in the temperature range from 100 °C to 400 °C, indicating that it possessed the most active adsorbed oxygen. Compared with the observation for Cu_2O-1 : 5, the first oxygen desorption peaks of Cu_2O-1 : 2 (185 °C) and Cu_2O-1 : 2.5 (128 °C) were observed at lower temperatures below 200 °C. Overall, the O_2-TPD results indicate that the oxygen mobility and storage in Cu_2O-1 : 2.5 are the highest among the three catalysts, which is beneficial to the release of intermediate adsorbed oxygen during the ozone decomposition process.

Oyama investigated the ozone decomposition mechanism,[49,50] and the process can be proposed as follows:

$$O_3 + * \rightarrow O_2 + O^{2-} \quad (1)$$

$$O_3 + O^{2-} \rightarrow O_2 + O_2^{2-} \quad (2)$$

$$O_2^{2-} \rightarrow O_2 + * \text{ (slow)} \quad (3)$$

Here, the symbol * represents an active site and step (3) represents the release of the intermediate adsorbed oxygen species from the surface active sites, which is the rate-determining step of ozone decomposition. XPS was conducted to detect the difference in the catalyst surface status before and after ozone

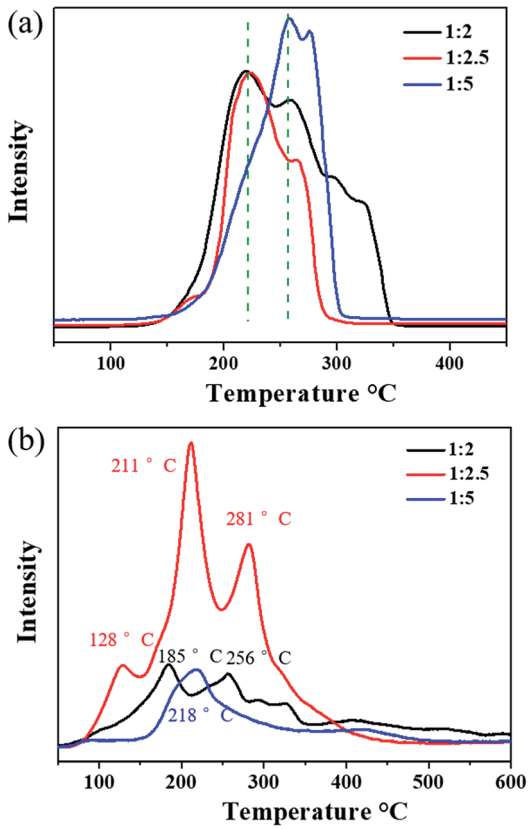

Fig. 5 (a) H_2-TPR and (b) O_2-TPD profiles of prepared Cu_2O samples.

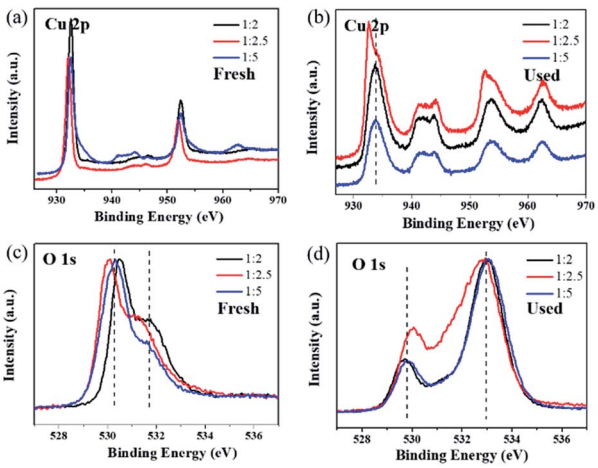

Fig. 6 XPS spectra of (a) Cu 2p, (b) O 1s in fresh samples, (c) Cu 2p and (d) O 1s in catalysts used in dry stream for 8 h.

decomposition in dry flow, as shown in Fig. 6. The peak located at 932.5 eV in the Cu 2p spectra (Fig. 6a) can be assigned to Cu $2p_{3/2}$ in Cu_2O.[51] After the ozone test, the Cu $2p_{3/2}$ binding energy of Cu_2O-1 : 2 and Cu_2O-1 : 5 shifted to a higher location at about 933.5 eV (shown in Fig. 6b). This suggests that the surface of Cu_2O is partially oxidized to CuO, which can also be verified by the shake-up satellite in the range of 940–945 eV in the Cu 2p spectra of the used catalysts.[52,53] To study the effect of CuO, the Cu_2O-1 : 2.5 catalyst was calcined in an air atmosphere at 600 °C for 2 h to obtain CuO, which, however, exhibited a poor ozone conversion efficiency of less than 10% during the 8 h test. Therefore, the active sites of ozone catalytic degradation might be the surface Cu(I) sites or some other crystal defects such as Cu vacancies, which made Cu_2O p-type. The first O 1s peak around 530.3 eV for the fresh samples can be assigned to the lattice oxygen of Cu_2O (Fig. 6c).[54] After testing for ozone decomposition, the peak of lattice oxygen slightly moved to a lower binding energy at around 529.7 eV (Fig. 6d), which could be attributed to the lattice oxygen of CuO.[55] Importantly, it was noticed that there was a broad peak in the high binding energy region of 531–534 eV in the O 1s spectra of the used catalysts. This peak at high binding energy can be ascribed to the chemisorbed oxygen species produced during the ozone decomposition process.[20] The ratio of surface adsorbed oxygen in the Cu_2O-1 : 2.5 catalyst was the lowest compared with that for Cu_2O-1 : 2 and Cu_2O-1 : 5 in the normalized O 1s spectra. The XPS results suggested that although some of the surface-active sites in Cu_2O-1 : 2.5 were occupied by the intermediate adsorbed oxygen species, the remaining highly active sites could still exhibit efficient ozone degradation. According to our previous work, the covering of surface-active sites by intermediate adsorbed oxygen is the main cause of Cu_2O catalyst deactivation, and the root reason for the highest ozone catalytic activity of the Cu_2O-1 : 2.5 catalyst is its smallest particle size, which is beneficial to the release of adsorbed oxygen.[31] This result is also consistent with that of O_2-TPD analysis.

As a proof-of-concept study for the application of the catalyst, Cu_2O nanoparticles were coated onto an Al honeycomb substrate to form a monolithic catalyst. Fig. 7a shows the photograph of the Cu_2O–Al honeycomb (diameter = 20 mm, thickness = 20 mm) coated by high-yield Cu_2O-1 : 2.5 (>20 g), where the active material on the Al honeycomb is about 0.2 g. The Cu_2O–Al honeycomb can decompose 10 ppm ozone completely for at least 24 h both in dry and high humidity conditions, as shown in Fig. 7a. In contrast, the Al honeycomb substrate alone exhibits relatively low catalytic activity of about 20–40% irrespective of whether it is coated with the Al_2O_3 sol. To further assess the potential of the catalyst, high-concentration ozone (3000 ppm) and high velocity (800 mL min^{-1}) were applied, and the conversion of 3000 ppm ozone over the Cu_2O–Al honeycomb was still nearly 100% (99.4%) after the 12 h test in dry flow with a space velocity of 8000 h^{-1}. Then, water vapor was added into the system; it was noticeable that although ozone conversion dropped slightly, it was still as high as 97.7% after the 24 h test, as shown in Fig. 7b. Overall, the high-output and highly active Cu_2O nanoparticles exhibit high catalytic performance and stability for ozone removal and display great potential for practical applications.

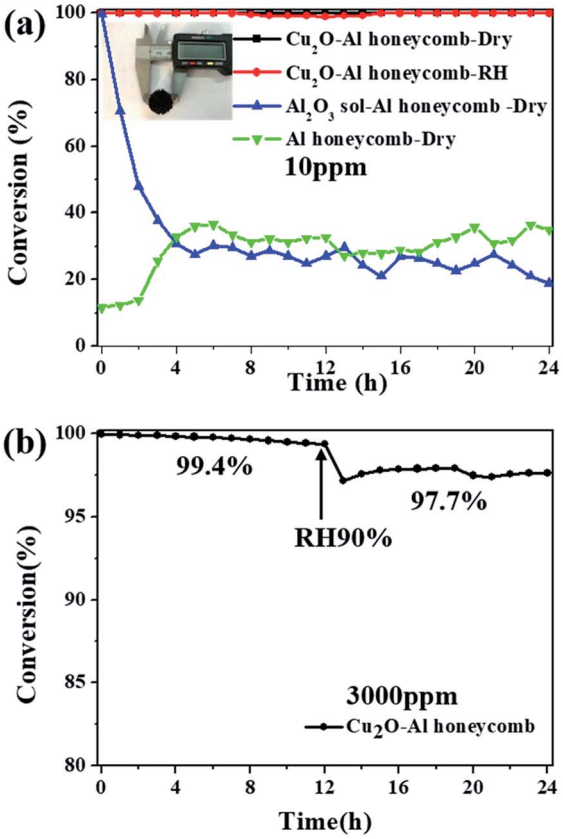

Fig. 7 (a) Photographs of Cu_2O–Al honeycomb and catalytic performance for the removal of low-concentration ozone (ozone inlet concentration: 10 ppm, $T = 25$ °C, gas flow = 200 mL min^{-1}, dry air or RH ~ 90%); (b) catalytic performance of fabricated Cu_2O–Al honeycomb for the removal of high-concentration ozone (ozone inlet concentration 3000 ppm, $T = 25$ °C, gas flow = 800 mL min^{-1}, space velocity 8000 h^{-1}, dry air or RH ~ 90%).

4. Conclusions

Cu_2O nanoparticles with high production of above 20 g and ultra-small size of several nanometers were successfully prepared through the facile reduction of Cu^{2+} by ascorbic acid in an alkaline solution at 25 °C. The ratio of Cu^{2+} : OH^- was the key parameter, which was optimized at 2.5. The as-synthesized Cu_2O showed complete removal for 1000 ppm ozone both under dry and high humidity conditions at 25 °C. For high-concentration 3000 ppm ozone, the conversion was 99.2% in dry flow and still above 95% in humid flow. The results of O_2-TPD and XPS suggested that the accumulation of intermediate oxygen species on the catalyst surface was the main cause for limiting ozone decomposition efficiency, and the small particle size of Cu_2O-1 : 2.5 was beneficial to its release. Moreover, a Cu_2O–Al honeycomb was fabricated and showed 99.4% and 97.7% ozone removal efficiency at dry and 90% RH conditions, respectively, at 3000 ppm and a space velocity of 8000 h^{-1}. These results show the promise of the simple strategy for producing high-yield Cu_2O for effective ozone elimination.

Conflicts of interest

There are no conflicts of interest to declare.

Acknowledgements

This research was financially supported by the National Key R&D Program of China (2016YFC0207100), the Strategic Priority Research Program of the Chinese Academy of Sciences (XDB05050400) and the State Key Laboratory of Multiphase Complex Systems (MPCS-2015-A-04).

Notes and references

1 R. Derwent, W. Collins, C. Johnson and D. Stevenson, *Environ. Sci. Technol.*, 2002, **36**, 379A–382A.
2 Q. Zhang, B. Yuan, M. Shao, X. Wang, S. Lu, K. Lu, M. Wang, L. Chen, C. C. Chang and S. C. Liu, *Atmos. Chem. Phys.*, 2014, **14**, 6089–6101.
3 K. Wałaszek, M. Kryza and M. Werner, *J. Atmos. Chem.*, 2018, **75**, 181–204.
4 D. A. Ikhlaq, *Desalin. Water Treat.*, 2019, **137**, 154–161.
5 Y. Shu, M. He, J. Ji, H. Huang, S. Liu and D. Y. C. Leung, *J. Hazard. Mater.*, 2019, **364**, 770–779.
6 H. Zhao, Y. Dong, P. Jiang, G. Wang, J. Zhang and K. Li, *Catal. Sci. Technol.*, 2014, **4**, 494–501.
7 R. Atkinson, *Atmos. Environ.*, 2000, **34**, 2063–2101.
8 C. Li, L. S. Balluz, A. Vaidyanathan, X.-J. Wen, Y. Hao and J. R. Qualters, *Medicine*, 2016, **95**, e2474.
9 V. J. Black, C. R. Black, J. A. Roberts and C. A. Stewart, *New Phytol.*, 2000, **147**, 421–447.
10 H. Wang, K. Lu, X. Chen, Q. Zhu, Q. Chen, S. Guo, M. Jiang, X. Li, D. Shang, Z. Tan, Y. Wu, Z. Wu, Q. Zou, Y. Zheng, L. Zeng, T. Zhu, M. Hu and Y. Zhang, *Environ. Sci. Technol. Lett.*, 2017, **4**, 416–420.
11 M. E. Jenkin and K. C. Clemitshaw, *Atmos. Environ.*, 2000, **34**, 2499–2527.
12 C. J. Weschler, *Environ. Health Perspect.*, 2006, **114**, 1489–1496.
13 Q. Yu, H. Pan, M. Zhao, Z. Liu, J. Wang, Y. Chen and M. Gong, *J. Hazard. Mater.*, 2009, **172**, 631–634.
14 P. Nikolov, K. Genov, P. Konova, K. Milenova, T. Batakliev, V. Georgiev, N. Kumar, D. K. Sarker, D. Pishev and S. Rakovsky, *J. Hazard. Mater.*, 2010, **184**, 16–19.
15 Z. Hao, D. Cheng, Y. Guo and Y. Liang, *Appl. Catal., B*, 2001, **33**, 217–222.
16 J. Jia, P. Zhang and L. Chen, *Catal. Sci. Technol.*, 2016, **6**, 5841–5847.
17 S. Liu, J. Ji, Y. Yu and H. Huang, *Catal. Sci. Technol.*, 2018, **8**, 4264–4273.
18 J. Ji, Y. Fang, L. He and H. Huang, *Catal. Sci. Technol.*, 2019, **9**, 4036–4046.
19 Y. Yu, S. Liu, J. Ji and H. Huang, *Catal. Sci. Technol.*, 2019, **9**, 5090–5099.
20 S. Imamura, M. Ikebata, T. Ito and T. Ogita, *Ind. Eng. Chem. Res.*, 1991, **30**, 217–221.
21 S. T. Oyama, *Catal. Rev.*, 2000, **42**, 279–322.
22 D. Wang, M. Mo, D. Yu, L. Xu, F. Li and Y. Qian, *Cryst. Growth Des.*, 2003, **3**, 717–720.
23 W.-H. Ke, C.-F. Hsia, Y.-J. Chen and M. H. Huang, *Small*, 2016, **12**, 3530–3534.
24 J. C. Park, J. Kim, H. Kwon and H. Song, *Adv. Mater.*, 2009, **21**, 803–807.
25 L.-I. Hung, C.-K. Tsung, W. Huang and P. Yang, *Adv. Mater.*, 2010, **22**, 1910–1914.
26 Y. Chang, J. J. Teo and H. C. Zeng, *Langmuir*, 2005, **21**, 1074–1079.
27 X. Lan, J. Zhang, H. Gao and T. Wang, *CrystEngComm*, 2011, **13**, 633–636.
28 W. Chen, L. Li, Q. Peng and Y. Li, *Nano Res.*, 2012, **5**, 320–326.
29 M. D. Susman, Y. Feldman, A. Vaskevich and I. Rubinstein, *ACS Nano*, 2014, **8**, 162–174.
30 M. Pang and H. C. Zeng, *Langmuir*, 2010, **26**, 5963–5970.
31 S. Gong, W. Li, Z. Xie, X. Ma, H. Liu, N. Han and Y. Chen, *New J. Chem.*, 2017, **41**, 4828–4834.
32 C.-H. Kuo and M. H. Huang, *J. Am. Chem. Soc.*, 2008, **130**, 12815–12820.
33 K. Chen and D. Xue, *CrystEngComm*, 2012, **14**, 8068–8075.
34 F. Meng and S. Jin, *Nano Lett.*, 2012, **12**, 234–239.
35 H. Wang, P. Rassu, X. Wang, H. Li, X. Wang, X. Wang, X. Feng, A. Yin, P. Li, X. Jin, S.-L. Chen, X. Ma and B. Wang, *Angew. Chem.*, 2018, **130**, 16654–16658.
36 Y. Liu, P. Zhang, J. Zhan and L. Liu, *Appl. Surf. Sci.*, 2019, **463**, 374–385.
37 J. Ma, C. Wang and H. He, *Appl. Catal., B*, 2017, **201**, 503–510.
38 J. Jia, P. Zhang and L. Chen, *Appl. Catal., B*, 2016, **189**, 210–218.
39 G. Zhu, J. Zhu, W. Li, W. Yao, R. Zong, Y. Zhu and Q. Zhang, *Environ. Sci. Technol.*, 2018, **52**, 8684–8692.
40 Y. Liu, W. Yang, P. Zhang and J. Zhang, *Appl. Surf. Sci.*, 2018, **442**, 640–649.
41 T. Gopi, G. Swetha, S. Chandra Shekar, C. Ramakrishna, B. Saini, R. Krishna and P. V. L. Rao, *Catal. Commun.*, 2017, **92**, 51–55.
42 Z. Lian, J. Ma and H. He, *Catal. Commun.*, 2015, **59**, 156–160.
43 W.-X. Tang, H.-D. Liu, X.-F. Wu and Y.-F. Chen, *Ozone: Sci. Eng.*, 2014, **36**, 502–512.
44 N. Kumar, P. M. Konova, A. Naydenov, T. Heikillä, T. Salmi and D. Y. Murzin, *Catal. Lett.*, 2004, **98**, 57–60.
45 S. Gong, Z. Xie, W. Li, X. Wu, N. Han and Y. Chen, *Appl. Catal., B*, 2019, **241**, 578–587.
46 Z. Zhang, H. Che, G. Jiajian, Y. Wang, X. She, J. Sun, P. Gunawan, Z. Zhong and F. Su, *Catal. Sci. Technol.*, 2012, **2**, 1207–1212.
47 Z. Fei, P. Lu, X. Feng, B. Sun and W. Ji, *Catal. Sci. Technol.*, 2012, **2**, 1705–1710.
48 S. Sun, D. Mao and J. Yu, *J. Rare Earths*, 2015, **33**, 1268–1274.
49 W. Li, G. V. Gibbs and S. T. Oyama, *J. Am. Chem. Soc.*, 1998, **120**, 9041–9046.
50 W. Li and S. T. Oyama, *J. Am. Chem. Soc.*, 1998, **120**, 9047–9052.
51 L. Zhang, D. Jing, L. Guo and X. Yao, *ACS Sustainable Chem. Eng.*, 2014, **2**, 1446–1452.

52 W. Shi, X. Guo, C. Cui, K. Jiang, Z. Li, L. Qu and J.-C. Wang, *Appl. Catal., B*, 2019, **243**, 236–242.
53 D. Zhang, B. Wang, X. Gong, Z. Yang and Y. Liu, *Chem. Eng. J.*, 2019, **359**, 1195–1204.
54 A. Chakravarty, K. Bhowmik, A. Mukherjee and G. De, *Langmuir*, 2015, **31**, 5210–5219.
55 X. Guo and R. Zhou, *Catal. Sci. Technol.*, 2016, **6**, 3862–3871.